Terahertz conductivity of localized photoinduced carriers in a Mott insulator $YTiO_3$ at low excitation density, contrasted with the metallic nature in a band semiconductor Si

2007 J. Phys.: Condens. Matter 19 406224

(http://iopscience.iop.org/0953-8984/19/40/406224)

IOP PUBLISHING JOURNAL OF PHYSICS: CONDENSED MATTER

J. Phys.: Condens. Matter **19** (2007) 406224 (12pp) doi:10.1088/0953-8984/19/40/406224

Terahertz conductivity of localized photoinduced carriers in a Mott insulator $YTiO_3$ at low excitation density, contrasted with the metallic nature in a band semiconductor Si

J Kitagawa[1], Y Kadoya[1], M Tsubota[2], F Iga[1] and T Takabatake[1]

[1] Department of Quantum Matter, ADSM, Hiroshima University, 1-3-1 Kagamiyama, Higashi-Hiroshima 739-8530, Japan
[2] Synchrotron Radiation Research Unit, JAEA, Hyogo 679-5148, Japan

E-mail: jkita@hiroshima-u.ac.jp

Received 23 May 2007, in final form 29 August 2007
Published 21 September 2007
Online at stacks.iop.org/JPhysCM/19/406224

Abstract

We performed optical-pump terahertz-probe measurements of a Mott insulator $YTiO_3$ and a band semiconductor Si using a laser diode (1.47 eV) and a femtosecond-pulse laser (1.55 eV). Both samples possess long energy-relaxation times (1.5 ms for $YTiO_3$ and 15 μs for Si); therefore, it is possible to extract terahertz complex conductivities of photoinduced carriers under equilibrium. We observed highly contrasting behaviour—Drude conductivity in Si and localized conductivity possibly obeying the Jonscher law in $YTiO_3$. The carrier number at the highest carrier-concentration layer in $YTiO_3$ is estimated to be 0.015 per Ti site. Anisotropic conductivity of $YTiO_3$ is determined. Our study indicates that localized carriers might play an important role in the incipient formation of photoinduced metallic phases in Mott insulators. In addition, this study shows that the transfer-matrix method is effective for extracting an optical constant of a sample with a spatially inhomogeneous carrier distribution.

1. Introduction

Recent discoveries of photoinduced metallic phases in several Mott insulators [1–6] made us consider the strongly correlated electron physics from a new point of view. However, the optical properties of photoinduced carriers in Mott insulators are not well understood even at low excitation densities. Understanding these optical properties is a prerequisite to understanding the incipient creation of metallic phases. Drude response by itinerant carriers is observed in the case of band semiconductors with low excited-carrier density (10^{14}–10^{16} cm^{-3}) [7–10]. The comparison between the optical properties of photoinduced carriers at low excitation densities

in Mott insulators and those in band semiconductors would be important in gaining deeper insight into strongly correlated electron physics.

The detailed nature of various carrier conductions, exhibiting Drude or hopping conduction, can be well characterized in the terahertz (THz) regime [11–14]. Terahertz time-domain spectroscopy (THz-TDS) is a powerful tool for analysing terahertz conductivity $\tilde{\sigma}(\omega)$ $(= \sigma_1(\omega) + i\sigma_2(\omega))$. The remarkable advantage of THz-TDS is its simultaneous determination of both the real and imaginary parts of $\tilde{\sigma}(\omega)$, without using the Kramers–Kronig transformation [15]. The coherent nature of the THz pulse is also utilized to investigate photoinduced $\tilde{\sigma}(\omega)$ by, for instance, optical-pump THz-probe (OPTP) studies. Recent progress in THz technologies [16, 17] and the methodology of analysis [18–20] in OPTP experiments enable the evaluation of transient $\tilde{\sigma}(\omega)$ in many substances, such as semiconductors, high-T_c superconductors, liquids and organic materials [8, 21–31].

Because the OPTP method essentially detects non-equilibrium processes, such as surface recombination and carrier diffusion, the time dependence of a complicated spatial carrier distribution must be considered [8, 32]. This difficulty is avoided by using thin-film samples [21–24, 28, 31] where the optical-pump pulse penetrates, and by analysing the photoinduced phase as a layer with a homogeneous $\tilde{\sigma}(\omega)$ [8, 22, 24, 28, 33]. Furthermore, the extraction of $\tilde{\sigma}(\omega)$, varying quickly compared with the pulse width of THz-probe pulse, only seems possible within some restricted conditions [18–20]. Therefore, to analyse photoinduced $\tilde{\sigma}(\omega)$ for a wide variety of Mott insulators, free from the restrictions in sample preparation and analysis, we initially examined a nearly equilibrium state of photoexcited bulk material with a longer energy-relaxation time, τ. The photoexcitation of a material with longer τ creates a quasi-equilibrium state averaging over various non-equilibrium processes, making it easy to obtain the optical constants of the highest carrier-concentration region in the material.

Our analysis also required extracting the $\tilde{\sigma}(\omega)$ of materials with inhomogeneous carrier distributions in a more rigorous manner. One good candidate for accomplishing this is the transfer-matrix method, which expresses inhomogeneous carrier distribution by a multi-layer system. This method has been briefly commented on in the literature [8]. The promise that the transfer-matrix method can incorporate inhomogeneity is seen in the analyses of reflectivity in optical pump–probe studies [34, 35]. Although it is a versatile method, its effectiveness has not been discussed thoroughly, especially in THz-TDS studies.

In this study, we found that the τ of a Mott insulator $YTiO_3$ with a Mott gap of approximately 1 eV [36] is 1.5 ms at 1.47 eV photoexcitation. We characterized the photoinduced $\tilde{\sigma}(\omega)$ by comparing it with that of a band semiconductor Si with a bandgap of 1.1 eV [37]. We also present a more detailed discussion of the transfer-matrix method.

2. Experimental method

Single-crystalline samples of $YTiO_3$, with the orthorhombic perovskite $GdFeO_3$-type structure, were grown by the floating zone method [38]. The Si sample was commercial high-resistivity Si.

Photoconductivity was measured to assess τ. The light emitted from a multi-mode continuous wave (CW) laser diode (LD) with a photon energy of 1.47 eV was modulated and used for illuminating the sample under an electric field of about 0.3 kV cm^{-1}. The photocurrent I_{ph} flowing through a 100 Ω resistance, connected in series with the sample, was lock-in detected.

The OPTP experiment was performed by a transmission THz-TDS system described in detail elsewhere [39, 40]. The thicknesses of the platelet samples were 420 μm for $YTiO_3$ and 512 μm for Si. The optical pulses were generated by a mode-locked Ti–sapphire laser with a

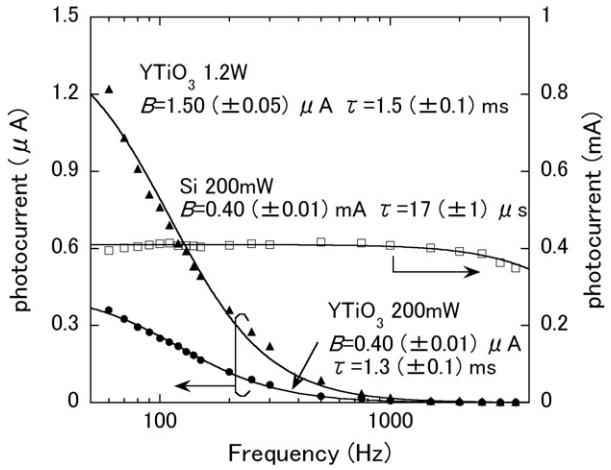

Figure 1. Photocurrent as a function of modulation frequency for Si and $YTiO_3$. The solid lines are $B/(1+(\omega\tau)^2)$ calculated with B and τ denoted in the figure.

repetition rate of 76 MHz and a central wavelength of 800 nm. Both the terahertz emitter and detector were low-temperature-grown GaAs photoconductive antennas. Si lenses were attached to the antennas to enhance the emission power and collection efficiency of THz pulses. The THz spectral range in this experiment was between 0.5 and 8 meV. The THz-wave-emission sides of the samples were photoexcited by the multi-mode CW LD with an incident angle of 45°. The pump-beam power was 0.8 W for Si and 1.2 W for $YTiO_3$. For $YTiO_3$, the polarization of the THz electric field E_{THz} is parallel to the b-axis. The beam diameter of the LD light was about 8 mm and was larger than that of the THz-probe pulse, which is energy dependent (e.g. 2 mm at 2 meV and 1 mm at 4 meV). The fluence rate was 1.6 W cm^{-2} for Si and 2.4 W cm^{-2} for $YTiO_3$, respectively. The temperature rise resulting from the thermalization by photoexcitation[3] is estimated not to exceed 1 K.

OPTP measurements were also performed with the 1.55 eV optical-pump pulses split from the Ti–sapphire laser to investigate the nature of conduction for carriers induced by light with a photon energy larger than that of the CW LD. This experiment studied the anisotropy of photoinduced $\tilde{\sigma}(\omega)$ in $YTiO_3$. The optical-pump pulse power was 230 mW. The optical-pump pulse beam diameter was about 2 mm (fluence: 96 nJ cm^{-2})—slightly smaller than that of the THz-probe pulse below 2 meV. The E_{THz} was applied along either the b-axis or the c-axis, maintaining the polarization of the optical-pump pulse electric field $E_{1.55\,\mathrm{eV}}$ parallel to the b-axis or the c-axis.

All measurements were performed at room temperature.

3. Results and discussion

Figure 1 shows the modulation-frequency dependence of I_{ph}. Increasing the modulation frequency causes I_{ph} to decrease, according to $\frac{B}{(1+(\omega\tau)^2)}$, where B is the proportional coefficient. The obtained B and τ are listed in the figure. Longer τ ($\sim$15 μs for Si and $\sim$1.5 ms for $YTiO_3$)

[3] The temperature rise ΔT_{s} under an equilibrium condition is calculated as follows. If all of the excitation power P is transformed into heat in a sample, ΔT_{s} is related to P by $\Delta T_{\mathrm{s}} = PL/S\kappa$, where L is the sample length, S is the illuminated area (see footnote 4) of 0.5 cm^2 and κ is the thermal conductivity of the sample (150 W m^{-1} K^{-1} for Si [37]). With the lack of κ data for $YTiO_3$, we employ an underestimated $\kappa = 10$ W m^{-1} K^{-1}.

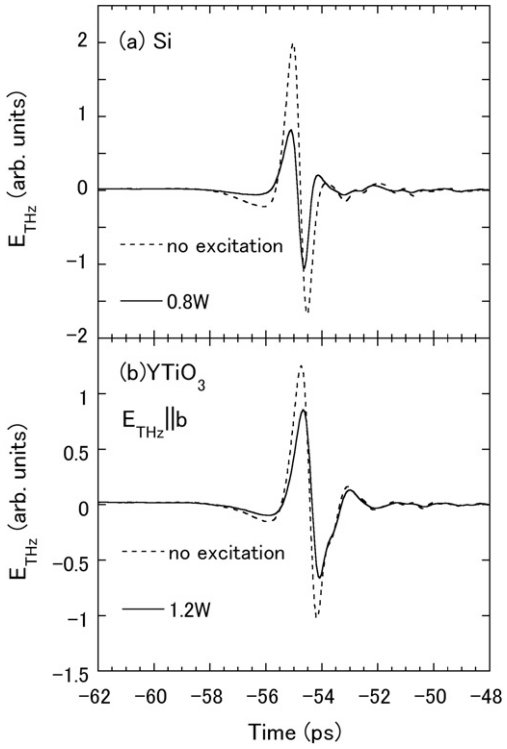

Figure 2. Time evolution of E_{THz} transmitted through (a) Si and (b) $YTiO_3$ with (solid lines) and without (broken lines) excitations (1.47 eV). The polarization of E_{THz} is parallel to the b-axis in $YTiO_3$. The excitation power is 0.8 W for Si and 1.2 W for $YTiO_3$.

indicate that the samples are in a quasi-equilibrium photoinduced state during the THz-TDS measurements. The τ of $YTiO_3$ is almost excitation-intensity independent; this implies that a thermal effect does not dominate the relaxation process. Although the direction of I_{ph} and of the electric field of the CW LD pump are not identified accurately in $YTiO_3$, a huge anisotropic τ that depends on the direction of I_{ph} and the polarization of the excitation light is not anticipated. The OPTP results shown later support this (see figure 7).

The temporal evolution of E_{THz} transmitted through Si and $YTiO_3$ are shown in figures 2(a) and (b), respectively, with and without LD excitations (1.47 eV). Photoexcitation attenuates both THz waves, implying that THz wave absorption is by the photoinduced carriers. The THz energy dependence of transmission $T(\omega)$ and phase shift $\Delta\phi(\omega)$ are obtained by Fourier transformation of the THz waves, as shown in figures 3(a) and (b). They are calculated using the equations $T(\omega) = \frac{E(\omega)}{E_{\mathrm{ref}}(\omega)}$ and $\Delta\phi(\omega) = \phi(\omega) - \phi_{\mathrm{ref}}(\omega)$, where $E(\omega)(E_{\mathrm{ref}}(\omega))$ and $\phi(\omega)(\phi_{\mathrm{ref}}(\omega))$ are the Fourier-transformed amplitude and phase, with and without excitation, respectively. THz wave absorption by photoinduced carriers is responsible for $T(\omega)$ decreasing below 1 for both samples, but the two exhibit different energy dependences. As the THz energy increases, the $T(\omega)$ of Si approaches 1, while that of $YTiO_3$ gradually decreases. The opposite sign of $\Delta\phi(\omega)$ for the two samples strongly indicates different fundamental conduction mechanisms for the photoinduced carriers. Negative (positive) $\Delta\phi$ roughly means that the refractive index is reduced (increased), compared with an unexcited state, which influences the negative (positive) real part of the dielectric constant of photoinduced carriers. As explained below, these results indicate a metallic nature below a plasma frequency in Si, and a localized nature, such as hopping carriers, in $YTiO_3$.

Before showing the photoinduced $\tilde{\sigma}(\omega)$ of Si and $YTiO_3$, we mention the detailed procedure of the transfer-matrix method. A spatially inhomogeneous distribution of

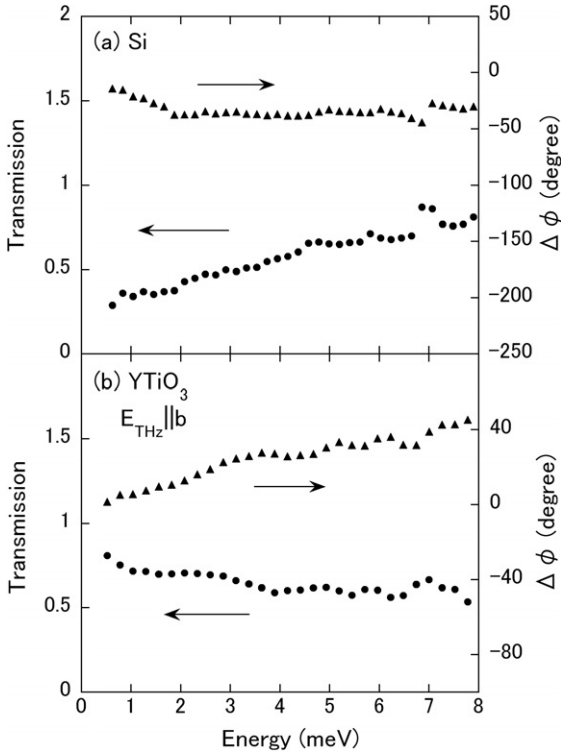

Figure 3. THz energy dependence of transmission and phase shift for (a) Si and (b) $YTiO_3$. The polarization of E_{THz} is parallel to the b-axis in $YTiO_3$.

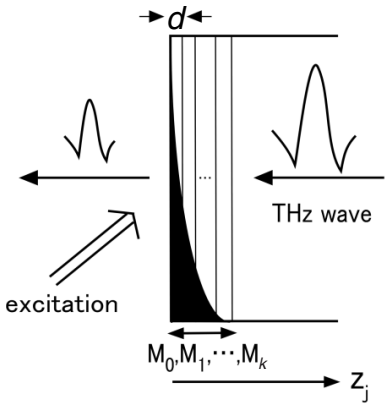

Figure 4. Illustration of a photoexcited sample to explain the transfer-matrix method. The coloured area demonstrates an exponentially decaying carrier density. The area is divided into many thin slabs with thickness d. The total number of thin slabs is k, and the transfer-matrix of each slab is expressed as M_j $(j = 0, 1, \ldots, k)$. The depth from the excited surface into the sample along the THz wave propagation is denoted as z_j.

photoinduced carriers is initially regarded as exponentially decaying. Subsequently, a non-exponentially decaying distribution is introduced. The photoinduced phase with an exponentially decaying carrier distribution is divided into many thin slabs (see figure 4). Each

slab is supposed to have a uniform complex refractive index $\tilde{n}_j$ whose value is set to reproduce the exponential decay of the photoinduced carrier concentration. The transfer-matrix of each slab is described by

$$M_j = \begin{pmatrix} \cos\delta & \mathrm{i}\sin\delta/\tilde{n}_j \\ \mathrm{i}\tilde{n}_j\sin\delta & \cos\delta \end{pmatrix}, \tag{1}$$

where j is the number index of the slab, $\delta = \frac{2\pi}{\lambda}\tilde{n}_j d$, λ is the incident THz wavelength in vacuum, and d is the slab thickness [41, 42]. The $\tilde{n}_j$ of each slab is calculated from the complex dielectric constant $\tilde{\epsilon}$ using,

$$\tilde{n}_j^2 = \tilde{\epsilon}_{\mathrm{no}} + \tilde{\epsilon}_{\mathrm{sur}}\exp\left(-\frac{z_j}{d_{\mathrm{p}}}\right), \tag{2}$$

where $\tilde{\epsilon}_{\mathrm{no}}$ is $\tilde{\epsilon}$ without excitation, $\tilde{\epsilon}_{\mathrm{sur}}$, the parameter to be optimized in this analysis is $\tilde{\epsilon}$ resulting from carriers at the photoexcited surface of the sample, z_j $(= j \times d)$ is the depth from the photoexcited surface into the sample along the THz wave propagation, and d_{p} is the optical penetration depth. For Si, a frequency-independent $\tilde{\epsilon}_{\mathrm{no}}$ [43] of 11.7 is used. For $YTiO_3$, $\tilde{\epsilon}_{\mathrm{no}}$ is determined experimentally from the THz-TDS measurement and is weakly energy dependent (e.g. $16.5 + 0.4\mathrm{i}$ at 2 meV and $17 + 0.4\mathrm{i}$ at 4 meV). d_{p} for Si at 1.47 eV is determined to be 8.4 μm using the absorption coefficient from an optical data handbook [44]. That for $YTiO_3$ at 1.47 eV was calculated to be 0.22 μm from the reported reflectivity spectra [45] (0.05–40 eV) combined with the Kramers–Kronig transformation. Then the total matrix M_{t} is described as

$$M_{\mathrm{t}} = \prod_{j=k}^{0} M_j, \tag{3}$$

where k is the total number of photoexcited slabs. Finally, the THz complex transmission is given by

$$T(\omega)\exp(\mathrm{i}\Delta\phi(\omega)) = \frac{t_{\mathrm{w}/LD}}{t_{\mathrm{wo}/LD}} = \frac{(Q + \mathrm{i}P)_{\mathrm{wo}/LD}}{(Q + \mathrm{i}P)_{\mathrm{w}/LD}}, \tag{4}$$

where $t_{\mathrm{w}/LD}$ and $t_{\mathrm{wo}/LD}$ mean the THz wave transmission with and without excitation, respectively, $Q = \mathrm{Re}((M_{\mathrm{t}11} + M_{\mathrm{t}12})\sqrt{\tilde{\epsilon}_{\mathrm{no}}} + M_{\mathrm{t}21} + M_{\mathrm{t}22})$ and $P = \mathrm{Im}((M_{\mathrm{t}11} + M_{\mathrm{t}12})\sqrt{\tilde{\epsilon}_{\mathrm{no}}} + M_{\mathrm{t}21} + M_{\mathrm{t}22})$. The fitting of experimental $T(\omega)$ and $\Delta\phi(\omega)$ following the above-mentioned procedure provides $\tilde{\sigma}(\omega)$ resulting from carriers at the photoexcited surface through

$$\tilde{\sigma}(\omega) = \mathrm{i}\omega\epsilon_0\tilde{\epsilon}_{\mathrm{sur}}(\omega), \tag{5}$$

where ϵ_0 is the vacuum permittivity. Note that the convergence of transmission is checked carefully by decreasing the thickness or by increasing the number of slabs. A thickness of the photoexcited phase $(= k \times d, k = 100)$ 5–10 times thicker than d_{p} is typically employed.

Figure 5 shows the photoinduced $\tilde{\sigma}(\omega)$ of Si and $YTiO_3$. $\tilde{\sigma}(\omega)$ for Si can be interpreted by the Drude model as

$$\sigma(\omega) = \frac{n_{\mathrm{c}} e\mu}{1 - \mathrm{i}\omega/\Gamma}, \tag{6}$$

$$\mu = \frac{e}{m^*\Gamma}, \tag{7}$$

where n_{c} is the carrier density, μ is the mobility, Γ is the carrier collision rate and m^* is the effective mass. The photoexcitation introduces both electrons and holes; therefore, the tentatively assigned value of m^* is $0.26m_0$ for electrons and $0.37m_0$ for holes [43], where m_0 is the free-electron mass. Hereafter, μ for each carrier is denoted as μ_{e} for electrons and μ_{h} for holes. We have considered the following two cases, neither of which can be excluded at

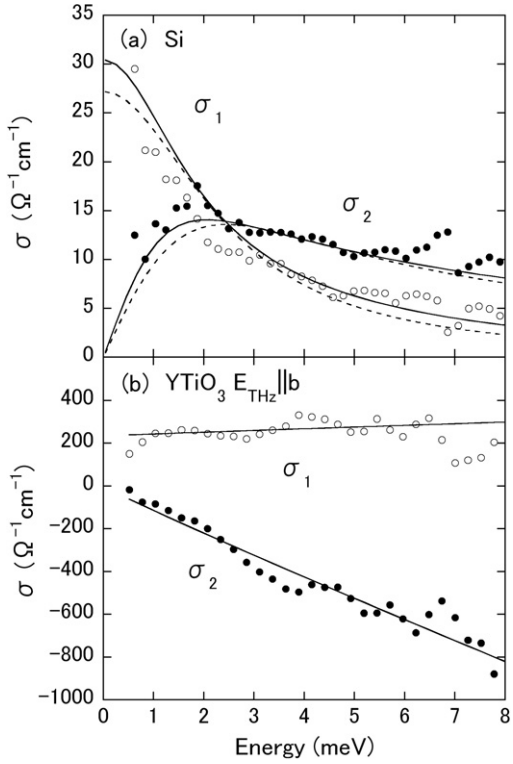

Figure 5. THz complex conductivity of (a) Si and (b) $YTiO_3$ at the photoexcited surface. The real and imaginary parts of conductivity correspond to σ_1 and σ_2, respectively. The solid and broken curves in (a) are $\tilde{\sigma}(\omega)$ calculated by the Drude models with $n_c = 6.6(\pm 0.3) \times 10^{16}$ cm^{-3}, $\mu_e = 2410(\pm 210)$ cm^2 V^{-1} s^{-1} and $\mu_h = 500(\pm 90)$ cm^2 V^{-1} s^{-1} for the solid curves (two-carrier model of electrons and holes), and with $n_c = 9.3(\pm 0.4) \times 10^{16}$ cm^{-3} and $\mu_e = 1820(\pm 100)$ cm^2 V^{-1} s^{-1} for the broken curves (only electrons under consideration), respectively. In the two-carrier model, the same n_c is assumed for each carrier. The solid curves in (b) are calculated $\tilde{\sigma}(\omega)$ using the Jonscher law with $\sigma_{dc} = 235(\pm 10)\ \Omega^{-1}$ cm^{-1}, $A = 2.40(\pm 0.05) \times 10^{-11}\ \Omega^{-1}$ cm^{-1} s$^{0.95}$ and $s = 0.95$.

the present stage. One is the two-carrier model of electrons and holes. The other takes only electrons into consideration, assuming that holes with heavy m^* do not contribute to $\tilde{\sigma}(\omega)$. The solid lines in figure 5(a) represent the calculated $\tilde{\sigma}(\omega)$ for the two-carrier model, and the broken lines represent the electron-only model. The curves are in agreement with the experimental $\tilde{\sigma}(\omega)$. This suggests that the itinerant carriers are certainly photogenerated in Si. The obtained μ_e and μ_h are $2410(\pm 210)$ cm^2 V^{-1} s^{-1} and $500(\pm 90)$ cm^2 V^{-1} s^{-1} for the two-carrier model, and μ_e is $1820(\pm 100)$ cm^2 V^{-1} s^{-1} for the other model. They are roughly consistent with the literature values [37], but it is to be noted that μ_e in both models might be larger than the predicted ones. The ambiguity of m^* may be responsible for this deviation.

The most striking feature in $\tilde{\sigma}(\omega)$ for $YTiO_3$ is the negative σ_2. This suggests the existence of localized carriers [27, 39, 46], which is very different from Si. The localization may arise from the on-site strong Coulomb interaction between 3d electrons in $YTiO_3$. To explain $\tilde{\sigma}(\omega)$, we used the empirical Jonscher law [47], which expresses $\tilde{\sigma}(\omega)$ for many materials with hopping carriers. The Jonscher law is given by [47, 48]

$$\sigma_1(\omega) = \sigma_{dc} + A\omega^s, \tag{8}$$

$$\sigma_2(\omega) = -A\omega^s \tan\frac{s\pi}{2}, \tag{9}$$

where σ_{dc} is the dc conductivity, A is the proportional coefficient and s is restricted between 0 and 1. As shown in figure 5(b), the solid curves from the Jonscher law seem to agree with the experimental $\tilde{\sigma}(\omega)$. In the solid curves, s, σ_{dc} and A are 0.95, 235($\pm$ 10) Ω^{-1} cm^{-1} and 2.40($\pm$ 0.05) $\times$ 10^{-11} Ω^{-1} cm^{-1} s$^{0.95}$, respectively. The allowed s ranges from 0.91 to 0.99, and the corresponding σ_{dc} and A are 210($\pm$ 10) Ω^{-1} cm^{-1} and 1.41($\pm$ 0.03) $\times$ 10^{-10} Ω^{-1} cm^{-1} s$^{0.91}$, and 260($\pm$ 10) Ω^{-1} cm^{-1} and 1.43($\pm$ 0.03) $\times$ 10^{-12} Ω^{-1} cm^{-1} s$^{0.99}$, respectively.

Note that $\tilde{\sigma}(\omega)$ can also be fitted by a two-component model, such as the Drude–Lorentz model. The estimated photoinduced carrier number at the surface layer is about 0.015 per Ti site. Photoexcited $YTiO_3$ with the derived carrier density would be equivalent to chemically hole-doped $Y_{1-x}Ca_xTiO_3$ with x much less than the 0.1 given in [36]. The $\sigma_1(\omega)$ spectrum for $Y_{1-x}Ca_xTiO_3$ in this composition region is very different than a Drude response. Therefore, it would be difficult to expect a Drude component to exist. Clarifying this point might require broadband spectroscopic information obtained under photoexcitation or the temperature dependence of $\tilde{\sigma}(\omega)$.

Since long relaxation times, τ, are observed in both samples, a diffusion or a surface-recombination process, making the carrier distribution a non-exponential decay type, must be considered, and the analysis method modified. The carrier number $n(z)$ along the THz wave propagation in a quasi-equilibrium state is obtained using a one-dimensional diffusion equation [49] as follows:

$$\frac{\partial n(z,t)}{\partial t} = D\frac{\partial^2 n(z,t)}{\partial z^2} - \frac{n(z,t)}{\tau} + \delta(t)\exp\left(-\frac{z}{d_p}\right), \tag{10}$$

where $n(z,t)$ depends on the time t and the position z along the THz wave propagation, and $\delta(t)$ is the δ-function. D is the diffusion coefficient and is given by

$$D = \frac{\mu_{bi}k_B T_s}{|e|}, \tag{11}$$

where $1/\mu_{bi}$ is equal to $1/\mu_e + 1/\mu_h$, k_B is the Boltzmann constant and T_s is the sample temperature equal to 300 K. The solution [49] of equation (10) is

$$n(z,t) = \exp\left(-\frac{z^2}{4Dt}\right)\left\{\frac{1}{2}\left[f\left(\frac{\sqrt{Dt}}{d_p} - \frac{z}{2\sqrt{Dt}}\right) + \frac{\frac{D}{d_p} + v_s}{\frac{D}{d_p} - v_s} f\left(\frac{\sqrt{Dt}}{d_p} + \frac{z}{2\sqrt{Dt}}\right)\right]\right.$$
$$\left. - \frac{v_s}{\frac{D}{d_p} - v_s} f\left(v_s\sqrt{\frac{t}{D}} + \frac{z}{2\sqrt{Dt}}\right)\right\}\exp\left(-\frac{t}{\tau}\right), \tag{12}$$

where v_s is the surface-recombination velocity and $f(z)$ is related to the error function by $f(z) = \exp(z^2)(1 - \mathrm{erf}(z))$. The carrier number in the quasi-equilibrium state requires the integration of $n(z,t)$ with respect to t,

$$n(z) = \int_0^\infty n(z,t)\,\mathrm{d}t. \tag{13}$$

Therefore, with the assumption of a conduction model and the knowledge of $n(z)$ determined by appropriate μ_{bi} and v_s, $T(\omega)e^{i\Delta\phi(\omega)}$ can be calculated using equation (4). In this case, equation (2) is replaced by

$$\tilde{n}_j^2 = \tilde{\epsilon}_{no} + \tilde{\epsilon}_{max}\frac{n(z_j)}{n_{max}}, \tag{14}$$

where n_{max} and $\tilde{\epsilon}_{max}$ are the $n(z)$ and $\tilde{\epsilon}$ of the highest carrier-concentration layer, respectively.

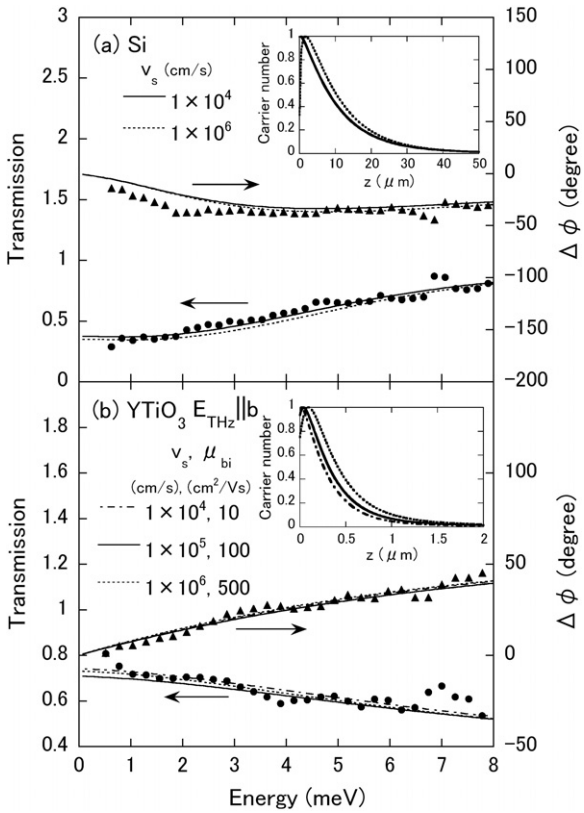

Figure 6. THz energy dependence of transmission and phase shift for (a) Si and (b) $YTiO_3$ analysed using the model with non-exponential carrier-distribution decay. The evaluated parameters v_s and μ_{bi} are listed in the figure. In (a), Drude conductivity characterized by $n_c = 5.2(\pm 0.3) \times 10^{16}$ cm^{-3} and the literature values of $\mu_e = 1500$ cm^2 V^{-1} s^{-1} and $\mu_h = 450$ cm^2 V^{-1} s^{-1} are assumed. The conduction model employed in (b) is the Jonscher law ($s = 0.95$), where σ_{dc} in Ω^{-1} cm^{-1} and A in Ω^{-1} cm^{-1} s$^{0.95}$ are $125(\pm 10)$ and $1.40(\pm 0.05) \times 10^{-11}$, $125(\pm 10)$ and $1.2(\pm 0.1) \times 10^{-11}$, and $90(\pm 10)$ and $1.0(\pm 0.1) \times 10^{-11}$ for the dotted–solid, solid and broken curves, respectively. The insets of (a) and (b) show z dependences of the carrier numbers normalized at n_{max}.

After the determination of μ_{bi} for Si (=346 cm^2 V^{-1} s^{-1}) using the literature values [37], v_s is varied between 1×10^4 and 1×10^6 cm s^{-1}. Representative $n(z)$ normalized at n_{max} are shown in the inset of figure 6(a). The n_{max} is observed around 1–2 μm. Assuming that both electrons and holes obeying the Drude conductivity are responsible for $\tilde{\sigma}(\omega)$, $T(\omega)e^{i\Delta\phi(\omega)}$ is confirmed as being consistent with experimental data for both $n(z)$ (see figure 6(a)). The estimated n_c is $5.2(\pm 0.3) \times 10^{16}$ cm^{-3} and is comparable to that obtained by the previous model. This indicates that, at the highest carrier-concentration layer, almost the same n_c can be obtained, irrespective of the carrier distribution decay type. For $YTiO_3$, both v_s and μ_{bi} are unknown parameters. The wide-range sweep of v_s and μ_{bi} gives various $n(z)$ curves as depicted in the inset of figure 6(b) with peak positions around 0.1 μm. For each $n(z)$, the experimental $T(\omega)e^{i\Delta\phi(\omega)}$ is well reproduced by the Jonscher law, where s is restricted within the same range obtained in figure 5(b) (0.91–0.99). Typical examples are shown in figure 6(b) with an s of 0.95. The other parameters (σ_{dc} in Ω^{-1} cm^{-1} and A in Ω^{-1} cm^{-1} s$^{0.95}$) for the dotted–solid, solid and broken lines are $125(\pm 10)$ and $1.40(\pm 0.05) \times 10^{-11}$, $125(\pm 10)$ and

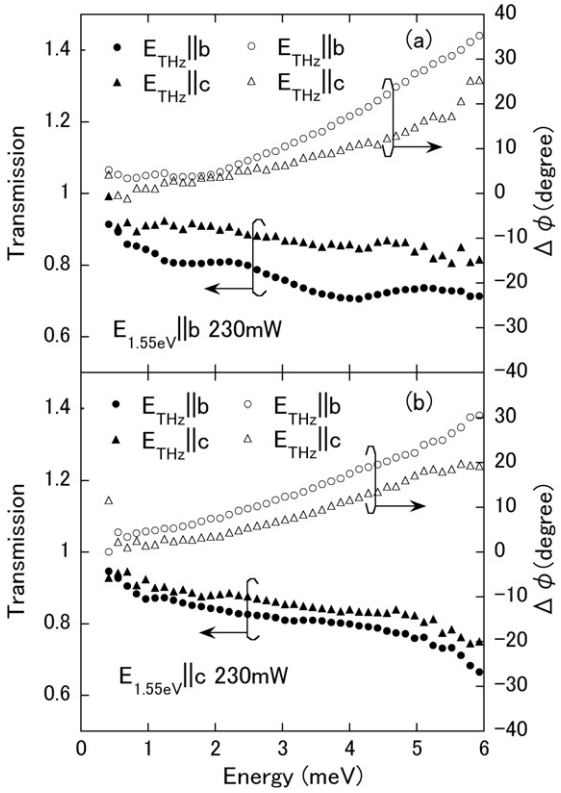

Figure 7. THz energy dependence of transmission and phase shift of $YTiO_3$ obtained from OPTP experiments, using a femtosecond-pulse laser (1.55 eV) under $E_{\mathrm{THz}} \parallel b$ and $E_{\mathrm{THz}} \parallel c$ for (a) $E_{1.55\,\mathrm{eV}} \parallel b$ and (b) $E_{1.55\,\mathrm{eV}} \parallel c$. The power of the optical-pump pulse is 230 mW.

$1.2(\pm 0.1) \times 10^{-11}$, and $90(\pm 10)$ and $1.0(\pm 0.1) \times 10^{-11}$, respectively. $\sigma_1(\omega)$ and $\sigma_2(\omega)$ calculated from the parameters are half to two-thirds of those in figure 5(b). Thus, for $YTiO_3$, the $\tilde{\sigma}(\omega)$ extracted from the model with an exponentially decaying carrier distribution roughly represents the highest carrier-concentration layer in the model using equation (14).

The photoinduced carrier number at the highest carrier-concentration layer in $YTiO_3$ is calculated as 0.015 per Ti site[4]. It can be proposed, therefore, that a phase with localized carriers would emerge initially at the photogeneration of the metallic phase in Mott insulators. Photoexcitation creates both electrons and holes, which differs from chemical doping, and a comparison of $\tilde{\sigma}(\omega)$ between photoexcited $YTiO_3$ and hole-doped $Y_{1-x}Ca_xTiO_3$ is discussed. The absolute value of $\sigma_1(\omega)$ for a photoexcited state might be much larger than that of the corresponding $Y_{1-x}Ca_xTiO_3$ if the extrapolation of $\sigma_1(\omega)$ in $Y_{1-x}Ca_xTiO_3$ is carried out toward the THz energy. The preservation of spectral weight implies that the localization energy of photoinduced carriers would be much lower than for holes in $Y_{1-x}Ca_xTiO_3$, even if both holes and electrons contribute to $\tilde{\sigma}(\omega)$ in photoexcited $YTiO_3$. As it is not clear that the large

[4] The photoinduced carrier density n_{c} at P is tentatively expressed by $n_{\mathrm{c}} = \frac{1}{1-\mathrm{e}^{-\hbar\omega/P\tau}} \times F \times \frac{1}{S \cdot d_{\mathrm{eff}}}$, where the first term indicates the carrier accumulation resulting from longer τ at photon energy $\hbar\omega$ of 1.47 eV, and the second term is the Fresnel loss (∼0.8 for $YTiO_3$ and ∼0.7 for Si). d_{eff} means the effective d_{p}, defined by $\int_0^\infty n(z)\,\mathrm{d}z/n_{\max}$, and is equal to 13 μm for Si and 0.55 μm for $YTiO_3$. This equation is initially applied to the experimental result for Si (figure 6(a)) with $n_{\mathrm{c}} = 5.2 \times 10^{16}$ cm^{-3}, in which S is determined to be 0.5 cm^2. Using the S, the carrier number for $YTiO_3$ can be derived.

difference in localization energy originates from only holes in such a low-carrier system, it is plausible that electrons with small localization energies also contribute to $\tilde{\sigma}(\omega)$. Therefore $\tilde{\sigma}(\omega)$ for photoexcited $YTiO_3$ would be supported by bound electrons as well as holes.

In a halogen-bridged Ni one-dimensional chain compound $[Ni(chxn)_2Br]Br_2$ (chxn = cyclohexanediamine), which is compared with $YTiO_3$ composed of a three-dimensional Ti network, the localized σ_1 is determined at a lower excitation density [3]. Despite being in a different energy region, carrier localization in photoexcited Mott insulators at low excitation densities may be the general phenomenon, irrespective of the dimensionality.

The fact that one-dimensional Mott insulators, such as $[Ni(chxn)_2Br]Br_2$ [3] and Sr_2CuO_3 [50], exhibit a τ in the order of picoseconds may suggest that dimensionality is a decisive factor for τ.

Figure 7 shows $T(\omega)$ and $\Delta\phi(\omega)$ obtained by OPTP experiments using a femtosecond-pulse laser (1.55 eV) for $YTiO_3$. Since the period of optical-pump arrival time (13 ns) is much shorter than τ, the photoinduced carriers are also in a quasi-equilibrium state. In both polarizations of $E_{1.55\,eV}$, it is found that the degree of variation in THz wave amplitude and phase from the unexcited state is larger for $E_{THz} \parallel b$ within the measured THz energy range. This implies that the absolute values of σ_1 and σ_2 for $E_{THz} \parallel b$ are larger than those for $E_{THz} \parallel c$. The anisotropy would reflect the crystal symmetry of $YTiO_3$ or the 3d-orbital state at the Ti site. Comparing the OPTP results to those using the CW LD, the $\tilde{\sigma}(\omega)$ does not seem to depend strongly on the optical-photon energy.

4. Summary

We have optically characterized photoinduced carriers for the Mott insulator $YTiO_3$ at low excitation densities in the THz regime using OPTP measurements, and compared the experimental results with those for band semiconductor Si. The τ of the photoinduced carriers in $YTiO_3$ is about 1.5 ms. The inhomogeneous carrier distribution along the THz wave propagation can be treated accurately using the transfer-matrix method. This method successfully determined $\tilde{\sigma}(\omega)$ for the highest carrier-concentration layer under the quasi-equilibrium states. $YTiO_3$ shows localized $\tilde{\sigma}(\omega)$, possibly with the Jonscher law, whereas Si exhibits the Drude response. An anisotropic $\tilde{\sigma}(\omega)$ in $YTiO_3$ is determined. Our study demonstrates that localized carriers might play an important role in the incipient formation of metallic phases in photoexcited Mott insulators. Although the exact origin of the localization in $YTiO_3$ remains an open question, THz–TDS under photoexcitation with another photon energy or for another Mott insulator might provide the answer. We note here that a preliminary THz-TDS experiment for $YTiO_3$ excited by a CW LD of 1.9 eV also leads to localized $\tilde{\sigma}(\omega)$.

Acknowledgments

This work was supported by Casio Science Foundation, and the Strategic Information and Communications R&D Promotion Programme of the Ministry of Public Management, Home Affairs, Posts and Telecommunications, Japan.

References

[1] Miyano K, Tanaka T, Tomioka Y and Tokura Y 1997 *Phys. Rev. Lett.* **78** 4257
[2] Cavalleri A, Tóth C, Siders C W, Squier J A, Ráksi F, Forget P and Kieffer J C 2001 *Phys. Rev. Lett.* **87** 237401
[3] Iwai S, Ono M, Maeda A, Matsuzaki H, Kishida H, Okamoto H and Tokura Y 2003 *Phys. Rev. Lett.* **91** 057401
[4] Tajima N, Fujisawa J, Naka N, Ishihara T, Kato R, Nishio Y and Kajita K 2005 *J. Phys. Soc. Japan* **74** 511

[5] Chollet M, Guerin L, Uchida N, Fukaya S, Shimoda H, Ishikawa T, Matsuda K, Hasegawa T, Ota A, Yamochi H, Saito G, Tazaki R, Adachi S and Koshihara S 2005 *Science* **307** 86
[6] Perfetti L, Loukakos P A, Lisowski M, Bovensiepen U, Berger H, Biermann S, Cornaglia P S, Georges A and Wolf M 2006 *Phys. Rev. Lett.* **97** 067402
[7] Ralph S E, Chen Y, Woodall J and McInturff D 1996 *Phys. Rev.* B **54** 5568
[8] Beard M C, Turner G M and Schmuttenmaer C A 2000 *Phys. Rev.* B **62** 15764
[9] Shan J, Wang F, Knoesel E, Bonn M and Heinz T F 2003 *Phys. Rev. Lett.* **90** 247401
[10] Dakovski G L, Kubera B, Lan S and Shan J 2006 *J. Opt. Soc. Am.* B **23** 139
[11] van Exter M and Grischkowsky D 1990 *Appl. Phys. Lett.* **56** 1694
[12] Katzenellenbogen N and Grischkowsky D 1992 *Appl. Phys. Lett.* **61** 840
[13] Jeon T-I and Grischkowsky D 1997 *Phys. Rev. Lett.* **78** 1106
[14] Harimochi H, Kitagawa J, Ishizaka M, Kadoya Y, Yamanishi M, Matsuishi S and Hosono H 2004 *Phys. Rev.* B **70** 193104
[15] Grüner G 1998 *Millimeter and Submillimeter Wave Spectroscopy of Solids* (Berlin: Springer)
[16] Mittleman D 2003 *Sensing with Terahertz Radiation* (Berlin: Springer)
[17] Sakai K 2005 *Terahertz Optoelectronics* (Berlin: Springer)
[18] Kindt J T and Schmuttenmaer C A 1999 *J. Chem. Phys.* **110** 8589
[19] Němec H, Kadlec F and Kužel P 2002 *J. Chem. Phys.* **117** 8454
[20] Nienhuys H K and Sundström V 2005 *Phys. Rev.* B **71** 235110
[21] Averitt R D, Rodriguez G, Siders J L W, Trugman S A and Taylor A J 2000 *J. Opt. Soc. Am.* B **17** 327
[22] Huber R, Tauser F, Brodschelm A, Bichler M, Abstreiter G and Leitenstorfer A 2001 *Nature* **414** 286
[23] Averitt R D, Lobad A I, Kwon C, Trugman S A, Thorsmølle V K and Taylor A J 2001 *Phys. Rev. Lett.* **87** 017401
[24] Beard M C, Turner G M and Schmuttenmaer C A 2001 *J. Appl. Phys.* **90** 5915
[25] Knoesel E, Bonn M, Shan J and Heinz T F 2001 *Phys. Rev. Lett.* **86** 340
[26] Hegmann F A, Tykwinski R R, Lui K P H, Bullock J E and Anthony J E 2002 *Phys. Rev. Lett.* **89** 227403
[27] Turner G M, Beard M C and Schmuttenmaer C A 2002 *J. Phys. Chem.* B **106** 11716
[28] Demsar J, Averitt R D, Taylor A J, Kabanov V V, Kang W N, Kim H J, Choi E M and Lee S I 2003 *Phys. Rev. Lett.* **91** 267002
[29] Kaindl R A, Carnahan M A, Hägele D, Lövenlch R and Chemla D S 2003 *Nature* **423** 734
[30] Hendry E, Wang F, Shan J, Heinz T F and Bonn M 2004 *Phys. Rev.* B **69** 081101
[31] Kampfrath T, Perfetti L, Schapper F, Frischkorn C and Wolf M 2005 *Phys. Rev. Lett.* **95** 187403
[32] Gallant M I and van Driel H M 1982 *Phys. Rev.* B **26** 2133
[33] Schall M and Jepsen P U 2000 *Opt. Lett.* **25** 13
[34] Ma H M, Liu Y X, Fei Y and Li F M 1989 *J. Appl. Phys.* **65** 5031
[35] Okamoto H, Ishige Y, Tanaka S, Kishida H, Iwai S and Tokura Y 2004 *Phys. Rev.* B **70** 165202
[36] Taguchi Y, Tokura Y, Arima T and Inaba F 1993 *Phys. Rev.* B **48** 511
[37] Sze S M 1981 *Physics of Semiconductor Devices* (New York: Wiley–Interscience)
[38] Tsubota M, Iga F, Nakano T, Uchihira K, Kura S, Takemura M, Bando Y, Umeo K, Takabatake T, Nishibori E, Takata M, Sakata M, Kato K and Ohishi Y 2003 *J. Phys. Soc. Japan* **72** 3182
[39] Kitagawa J, Ishizaka M, Kadoya Y, Matsuishi S and Hosono H 2006 *J. Phys. Soc. Japan* **75** 084715
[40] Kitagawa J, Kadoya Y, Tsubota M, Iga F and Takabatake T 2007 *J. Magn. Magn. Mater.* **310** 913
[41] Born M and Wolf E 1980 *Principles of Optics* 6th edn (New York: Pergamon)
[42] Harimochi H, Kitagawa J, Kadoya Y and Yamanishi M 2004 *Japan. J. Appl. Phys.* **43** 7320
[43] van Exter M and Grischkowsky D 1990 *Phys. Rev.* B **41** 12140
[44] Palik E D 1985 *Handbook of Optical Constants of Solids* (New York: Academic)
[45] Okimoto Y, Katsufuji T, Okada Y, Arima T and Tokura Y 1995 *Phys. Rev.* B **51** 9581
[46] Cooke D G, MacDonald A N, Hryciw A, Wang J, Li Q, Meldrum A and Hegmann F A 2006 *Phys. Rev.* B **73** 193311
[47] Jonscher A K 1977 *Nature* **267** 673
[48] Elliott S R 1987 *Adv. Phys.* **36** 135
[49] Vaitkus J 1976 *Phys. Status Solidi* a **34** 769
[50] Ogasawara T, Ashida M, Motoyama N, Eisaki H, Uchida S, Tokura Y, Ghosh H, Shukla A, Mazumdar S and Kuwata-Gonokami M 2000 *Phys. Rev. Lett.* **85** 2204